Hindawi
Mathematical Problems in Engineering
Volume 2020, Article ID 4316921, 10 pages
https://doi.org/10.1155/2020/4316921

Research Article

Main Girder Deflection Variations in Cable-Stayed Bridge with Temperature over Various Time Scales

Dian Jin,[1] Xiaoling Liu,[1] Bing Wang,[2] and Qiao Huang[3]

[1]*Faculty of Maritime and Transportation, Ningbo University, Ningbo 315211, China*
[2]*School of Civil and Environmental Engineering, Ningbo University, Ningbo 315211, China*
[3]*School of Transportation, Southeast University, Nanjing 210096, China*

Correspondence should be addressed to Xiaoling Liu; liuxiaolingseu@163.com

Received 28 May 2020; Revised 23 July 2020; Accepted 8 August 2020; Published 26 August 2020

Academic Editor: Federico Guarracino

The cable-stay bridge is a complex hyperstatic structure with large span and slender proportions, making it highly sensitive to temperature, especially in terms of deformation. A cable-stayed bridge with a steel tower and steel box girder was taken as an example in this study to explore the temperature effects on the deflection of the main girder under different time scales. The temperature gradient characteristics of the girder and tower were observed; then, the daily and annual variations of girder deflection were investigated. Finally, the main influencing factors of deflection variations with temperature were verified by finite element simulation. The results show that the girder/pylon temperature gradient under current Chinese code is not applicable to cable-stayed bridges, and the measured values are usually underestimated. In terms of diurnal variations, the deflection is greatly affected by the temperature difference between the cable and beam and the temperature gradient of the girder. The annual variation law of deflection data and temperature at 1 : 00am shows obvious linear characteristics. The daily deflection at 1 : 00am., after removing the temperature effect, can thus be used as an index to evaluate the long-term degradation of bridges. This is a workable approach for efficient and rapid mining of large sets of monitoring data.

1. Introduction

Cable-stayed bridges are components of many transportation systems across the globe. They are popular as they are aesthetically pleasing and have strong mechanical and economic performance. Transportation infrastructure construction projects are booming in China, and at present, China has the world's largest number of cable-stayed bridges: approximately 60 with a total span of more than 200 meters [1]. Long-span cable-stayed bridges are often located in traffic throat positions and serve as important transportation hubs. Most are equipped with health monitoring systems to control their operation states; the deflection of the main girder is an important health monitoring parameter [2] as it reflects deformation in the bridge, which can indirectly reveal any abnormal displacement of the cable force, pylon, expansion joint, bearing, and other parts of the structure. Main girder deflection is of great significance for damage identification [3, 4]. The influence of temperature on bridge deformation is usually greater than that of traffic or wind loads. A benchmark model of temperature and deformation effects can be used to monitor changes in the structure's performance, which makes research on bridge temperature effects very valuable [5–7].

The temperature effects of high-order statically indeterminate structures are highly complex. Measurement results vary throughout the literature [8–12]. Five-day monitoring data of the Zhanjiang Bay Bridge in the summer of 2008 showed that the mid-span deflection of the main girder increased during the high-temperature period [13]. Lee et al. [14] found that the elevation of the Seohae Bridge girder in South Korea is higher in summer than in winter but did not explain the reason for this phenomenon. Monitoring data of the Donghai Bridge from March to September 2007 showed that mid-span deflection decreased with an increase in the average temperature over the main girder; a time lag

emerged between the deformation and the temperature as well [7]. Monitoring data for the Dafosi Yangtze River Bridge and Masongxi Yangtze River Bridge over an approximately 10-day period showed that the deck of the mid-span bridge dropped when temperature increased [15]. The relationship between main girder vertical displacement and temperature is not consistent in cable-stayed bridges, though this is the case in suspension bridges [16].

Many previous scholars have explored temperature actions via finite element analysis. Zhou et al. [17] investigated the effects of seasonal as well as diurnal temperature variations on thermally induced changes in the mid-span vertical displacement of steel bridges; they assessed the effects of the distance between the two tower tops and cable tensions based on monitoring data for steel box girder and twin-tower cable-stayed bridges. They found that the correlations between temperature and structural responses can be classified into two modes. Lucas et al. [18] processed temperature data for the steel box girder of the Normandy Bridge to determine the daily change rule of the girder temperature. Xia et al. [19] analyzed the factors influencing the temperature distributions of the Tsing Ma suspension bridge based on numerical simulation. Miao and Shi [20] proposed a temperature gradient for the hexagonal flat steel box girder. Zhou et al. [21] investigated the mechanisms of temperature effects on the mid-span vertical displacement of the Shanghai Yangtze River Bridge via plane geometric and finite element analyses.

Previous scholars have conducted in-depth analyses of the temperature effects of deflection in cable-stayed bridges of different materials, but there are few reports on temperature effects in cable-stayed bridges with steel towers and steel girders specifically. Additionally, there is no suitable evaluation index for the long-term deflection degradation of cable-stayed bridges. A cable-stayed bridge with a steel tower and steel main girder, the Nanjing No. 3 Yangtze River Bridge, was taken as an example in this study. The temperature field and girder deflection monitoring data were utilized to determine the temperature distribution patterns as per British and Chinese temperature gradient design specifications. The diurnal and annual variations in girder deflection with temperature were monitored accordingly, then verified according to a finite element simulation. Finally, the appropriate index was established to efficiently and accurately reflect the long-term structural degradation. The conclusions of this work may not only deepen our understanding of the temperature effects of steel cable-stayed bridges but also provide an approach for efficient and rapid mining of large quantities of monitoring data.

2. Temperature Characteristics Analysis of the Girder and Pylon

2.1. Introduction to the Monitoring System. The research object discussed in this paper is the Nanjing No. 3 Yangtze River Bridge, which is located in Nanjing City, Jiangsu Province, China (Figure 1). The bridge opened in October 2005. Its main structure is a cable-stayed bridge with a main span of 648 meters plus a tower 215 meters in height. It is a five-span, 1288 m long cable-stayed bridge structure with a span arrangement of 63 + 257+648 + 257 + 63. It is equipped with steel pylon, steel box girder, and reinforced concrete pier components. It was the first cable-stayed bridge with steel towers completed in China and the world's first cable-stayed bridge with an arc-shaped steel tower.

The bridge health monitoring system (BHMS) was put into use in May 2006. The system includes a sensor subsystem, data acquisition and transmission subsystem, data processing and control subsystem, structural safety evaluation subsystem, center database subsystem, user interface subsystem, and electronic inspection and maintenance management subsystem. The sensor subsystem continuously measures a number of bridge parameters related to the structures' response and environment (e.g., strain, cable force, geometric deformation, dynamic characteristics, and structural temperature). The system contains a total of 548 types of sensors. The specific number of relevant sensors targeting temperature and girder deflection is given in Table 1.

2.2. Temperature Distribution of Steel Box Girder. The vertical temperature gradient is an important temperature effect in the steel box girder, as it significantly affects the stress of the structure. The temperature gradient distribution assessed in this study is discussed in this section.

The main girder of the target bridge is a streamlined flat steel box girder 3.2 m in height and 37.2 m in width, comprised of Q345-D steel. The thickness of the bridge deck pavement is 50 mm. The standard girder (15 m length) contains four solid diaphragm plates spaced 3.75 m apart.

The temperature mode of each section in the longitudinal direction of a given bridge is basically consistent [21], so only one position is necessary for an effective analysis. Consider the mid-span monitoring points of the target bridge as an example; the temperature monitoring point arrangement is as shown in Figure 2. There are seven monitoring points in the top plate (GT1-GT7), four in the web plate (GW1-GW4), and five in the bottom plate (GB1-GB5).

The steel box girder provides temperature sensor data to the system every 30 min with 0.5°C precision. The transverse temperature distribution of the bottom plate and top plate is basically consistent, while there is a pronounced vertical temperature gradient. To obtain the maximum temperature gradient distribution for subsequent calculation of temperature effects, temperature data from days with the strongest solar radiation were collected. Monitoring data statistics for temperature differences throughout 2007 showed that July 26 was best-suited to this analysis; data from this day was abstracted accordingly.

GT1 (top plate) and GW1-2 (web plate) data were selected for analysis. The differences between them and the mean temperature of the bottom plate are shown in Figure 3. The maximum temperature difference occurred between 14 : 00 and 15 : 30. The mean values of temperature difference during this period can be considered as the data reference value of the maximum vertical temperature gradient, as marked with a "△" in Figure 4.

Figure 1: Picture of Nanjing No.3 Yangtze river bridge.

Table 1: Statistics of relevant sensor number.

Monitored item	Number on girder	Number on south tower	Number on north tower	Total
Temperature	172	36	36	244
Ambient temperature	4	4	4	12
Girder deflection	75	0	0	75

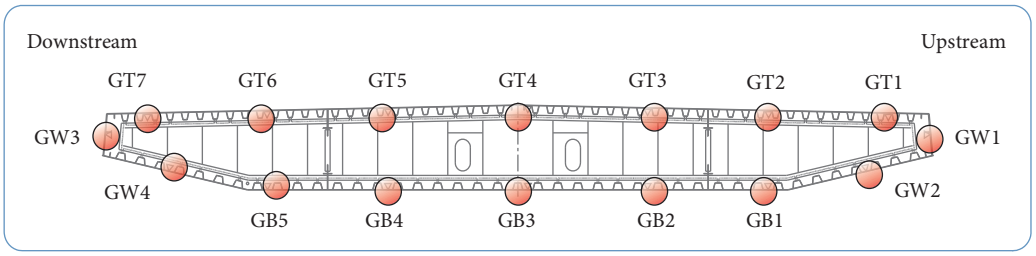

Figure 2: Temperature monitoring point arrangement in mid-span girder.

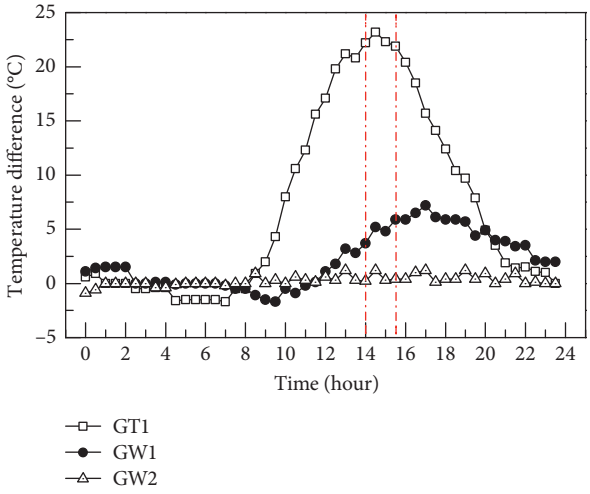

Figure 3: Temperature distributions of the vertical temperature gradient.

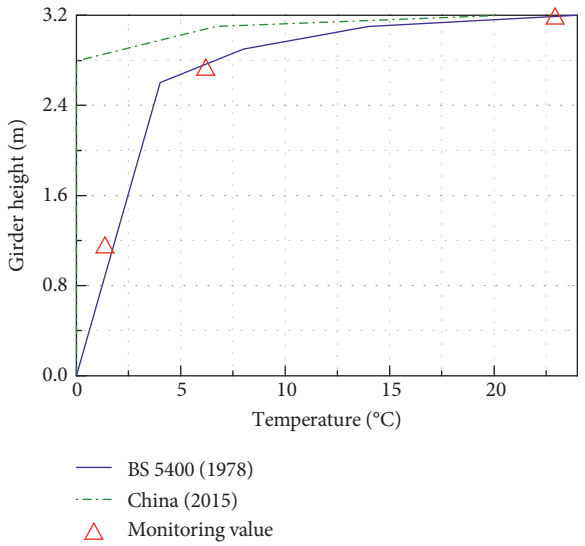

Figure 4: Fitted vertical temperature gradient of steel box girder on July 26, 2007.

The British standard BS5400 provides detailed regulation over bridge girder temperature effects [22]. The general specifications for the design of highway bridges and culverts (JTG D60-2015) in China have relatively simple regulation for calculating temperature effects in the T-section continuous beam [23]. Figure 4 also shows the temperature gradient distributions under both sets of specifications.

As shown in Figure 4, the main girder temperature gradient specified in China's codes cannot be directly applied to steel box girders in cable-stayed bridges. The monitoring value of this bridge basically conforms to the temperature gradient in the British code, however. The girder temperature gradient of British standard BS 5400 can thus be reasonably applied for finite element simulation purposes.

2.3. Temperature Distribution of Steel Pylon. The design codes of various countries lack information regarding the temperature gradient of the steel pylon. The temperature difference is 5°C in the codes given by China and Europe. The location of the pylon temperature monitoring point used in this study is given in Figure 5. The upstream and downstream measuring points are symmetrically arranged. Two measuring points are arranged at four corners in the box cell and numbered $P1$ to $P8$, respectively, across the monitoring points 40 m above the bridge deck.

Since the two temperature measuring points at each corner are almost entirely consistent, only one was chosen as a reference here. Figure 6 shows the temperature changes of the four measuring points of upstream $P8, P4, P1$ and $P5$. The resolution of the temperature sensor is 0.5 °C, so the curve has a stepped shape. $P1$ and $P4$ belong to the south side and $P5$ and $P8$ to the north side of the structure. Due to the angle at which solar radiation strikes the bridge, the temperature rises more quickly on the south side than the north; the maximum temperature difference of the steel tower occurs around 10 : 30, which is 3–5 hours ahead of the maximum temperature difference of the steel box girder. The maximum temperature difference is 6°C, which is slightly higher than the value given in the code.

We also found that the maximum negative temperature difference of the pylon occurred in winter, at 9.94 between 16 : 00 and 17 : 00 on January 7. This is much larger than the value given in the code of China or Europe. Therefore, the measurement data should be used to define the temperature gradient of the tower.

3. Variation Law Analysis of Girder Deflection under Different Time Scales

The deflection of the main girder of the cable-stayed bridge reflects the stress condition and potential damage to the entire structure. The deck alignment should generally be detected separately in the annual inspection. Through several years of monitoring data analysis, we discovered that changes in deflection have multiscale features with temperature variations. We divided these results into two scales

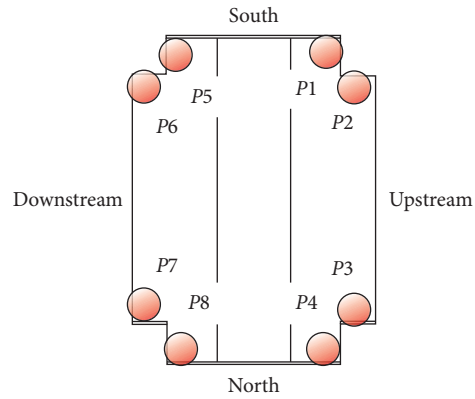

Figure 5: Temperature monitoring point arrangement in steel pylon.

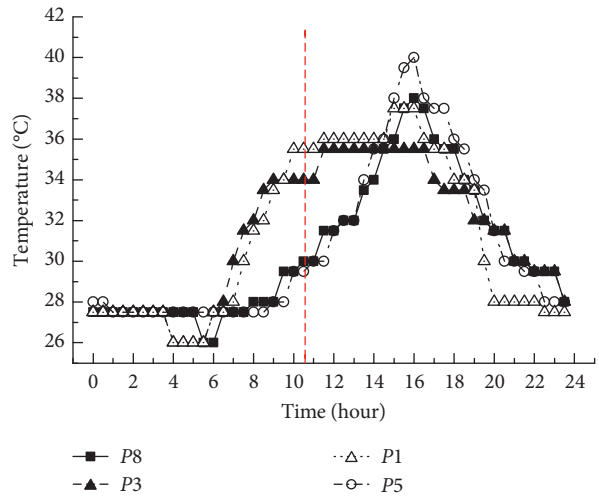

Figure 6: Curves of partial temperature sensors.

to create a daily temperature model and annual temperature model, as discussed in detail in the following.

3.1. Diurnal Variations. The main girder deflection monitoring process was conducted via a closed connected pipe method using a ROSEMOUNT 3051S, which has high precision, fast reaction, good synchronism, and high-frequency acquisition capability. The horizontality of the liquid surface in the connected pipe was exploited to connect the pipe along the beam, transfer the changes in liquid level over the pressure wave, and reveal fluctuations in liquid pressure by a high-performance pressure transmitter that could be converted into a numerical bridge deflection value. We found that the correlation between each measurement point was very high, so we focused only on the deflection of the mid-span.

The variations in mid-span deflection and temperature over a five-day period in 2007 are shown in Figure 7. Negative values indicate down-deflection and girder deflection at the pylon (0). As shown in Figure 7, the mid-span deflection fluctuated along with temperature and produced a "hysteresis loop" [24]. The temperature changes in one day

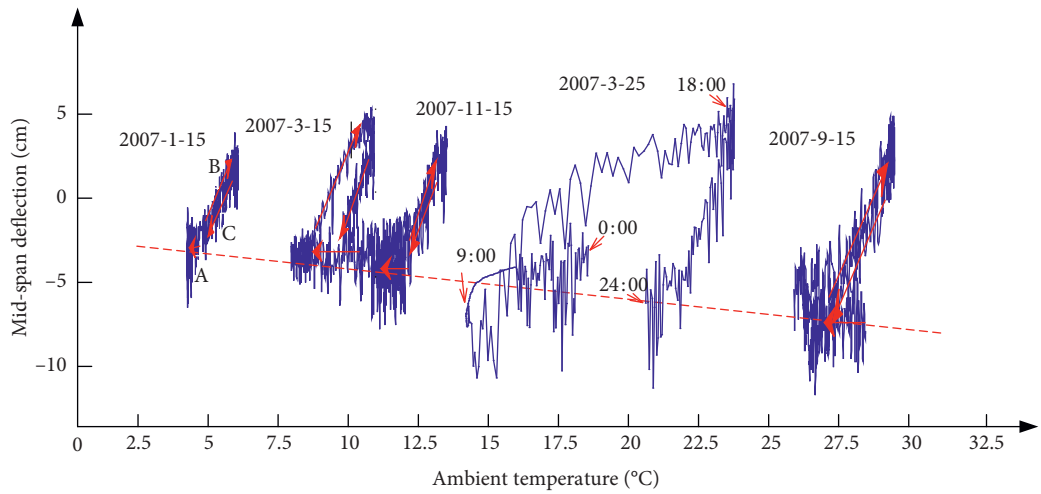

Figure 7: Change rules of mid-span deflection with temperature for five days in 2007.

were divided into three stages: temperature fall, temperature rise, and a secondary temperature fall. The three corresponding stages of mid-span deflection were labeled as A, B, and C, respectively. Stage A occurred from 0 : 00 to sunrise; as the structure was in a dark environment, the deflective effects of temperature were relatively small. The deflective effects of vehicle loads were larger at this time, likely due to the relatively high proportion of heavy vehicles in the nighttime hours. During Stage B, which occurred from sunrise to the sunset, the mid-span deflection decreased as temperature increased. The mid-span deflection gradually increased throughout Stage C, which occurred from sunset to 24 : 00.

The hysteresis loops gathered in this analysis also appear to be different sizes. We reached several conclusions regarding the typical temperature and deflection curves of the five-day period observed here:

(a) When the maximum temperature difference is large over the course of one day, the corresponding deflection change is large and the hysteresis loop is relatively large (and vice versa). When the maximum temperature difference over one day is small (which is common in summer and winter months), the relationship between deflection and temperature is nearly linear due to the limited range of solar radiation during the day. When the temperature difference in spring and autumn is large, the deflection shows a distinct and nonstationary change.

(b) The deflection change rate grows gradually stable at a certain value in Stage B. The fitting result based on monitoring data was approximately 4 cm/°C in this case. The mechanism behind this observation was determined via finite element simulation, as discussed in the following section.

(c) The mid-span deflection is relatively stable due to the stable ambient temperature during the period from 0 : 00 to sunrise. The red dotted line in Figure 7 roughly indicates that there is a negative correlation between the deflection and temperature at 1 : 00. The mid-span deflection at 1 : 00 can be used as the basic data for long-term trend analysis. Annual deflection variations can be obtained by collecting the data at 1 : 00, as discussed in detail in the following.

3.2. Annual Variations. Data from January 2007 to December 2009 (one day per month) were extracted to investigate annual variations. We collected the average mid-span deflection and temperature from 0 : 00 to 1 : 00 per day and plugged the data into a linear simulation. Figure 8 shows the changes in mid-span deflection with temperature, which have a strong negative correlation with a Pearson coefficient of −0.87. The linear fitting results were calculated as follows:where D is the average monitored mid-span deflection from 0 : 00 to 1 : 00 in a day in millimetres; T is the average monitored temperature from 0 : 00 to 1 : 00 in a day in degrees Celsius.

$$D = -1.721 \times T - 19.986, \quad (1)$$

The slope in the formula is −1.721, which indicates that the variation in mid-span deflection caused by unit temperature is −1.721. (This was also simulated by finite element analysis, as discussed below.) The girder deflection was unified to the same temperature during the completion of the bridge (24°C) through a linear fitting. The data accumulated and the damage appears to be easily verifiable. The maintenance department was recommended to conduct targeted inspections based on this damage data.

4. Finite Element Analysis

4.1. Finite Element Model Establishment. Theoretically, a model with relative accuracy can simulate the actual mechanical behavior of a given structure. The reliability of monitoring data can be verified through changes in cable forces and deflection as-acquired by exerting a corresponding temperature load in a finite element model. We built a spatial "fishbone-typed beam" model (Figure 9)

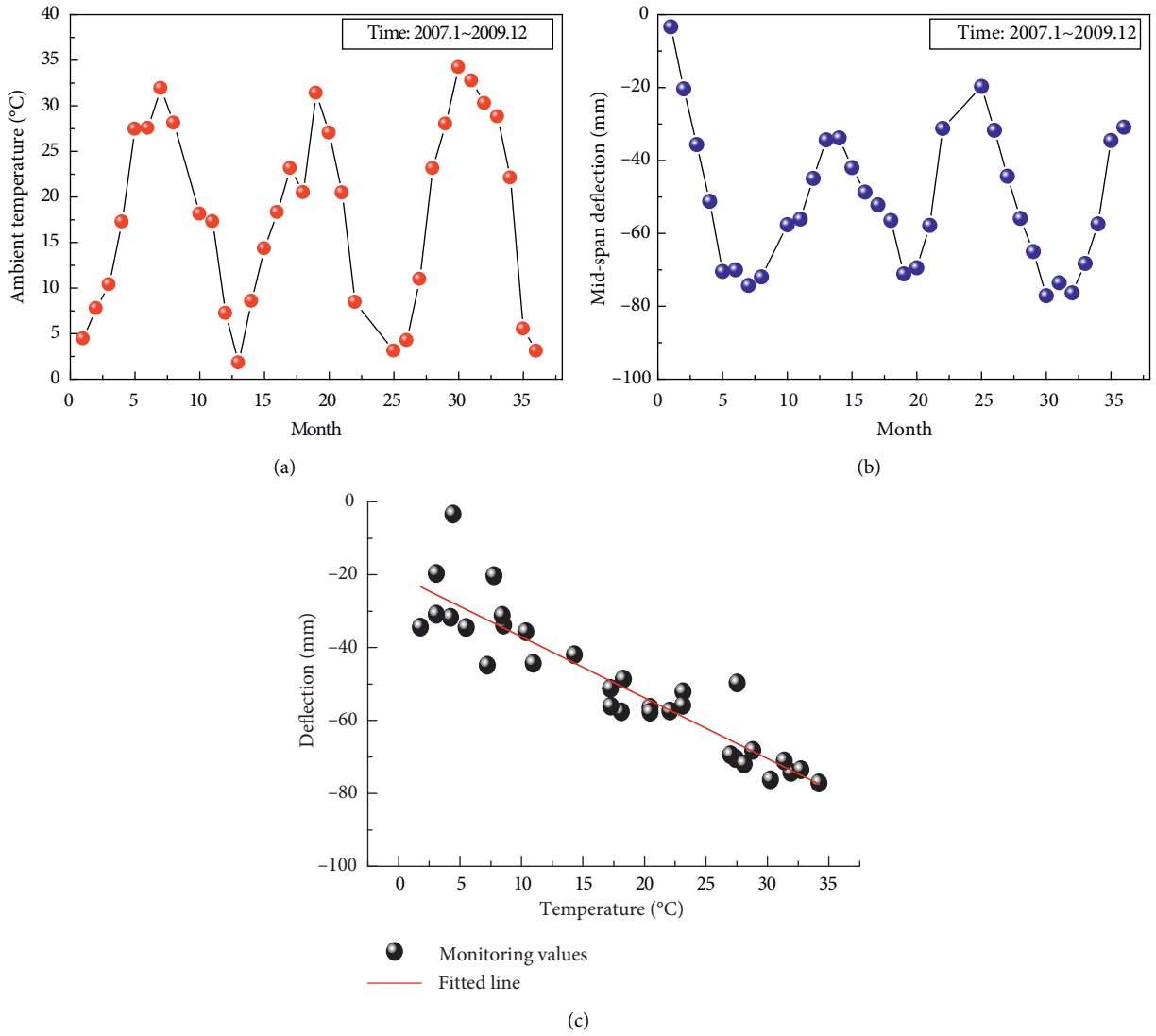

Figure 8: Data and linear fitting of mid-span deflection and temperature. (a) Ambient temperature data. (b) Mid-span deflection data. (c) Linear fitting of mid-span deflection and temperature.

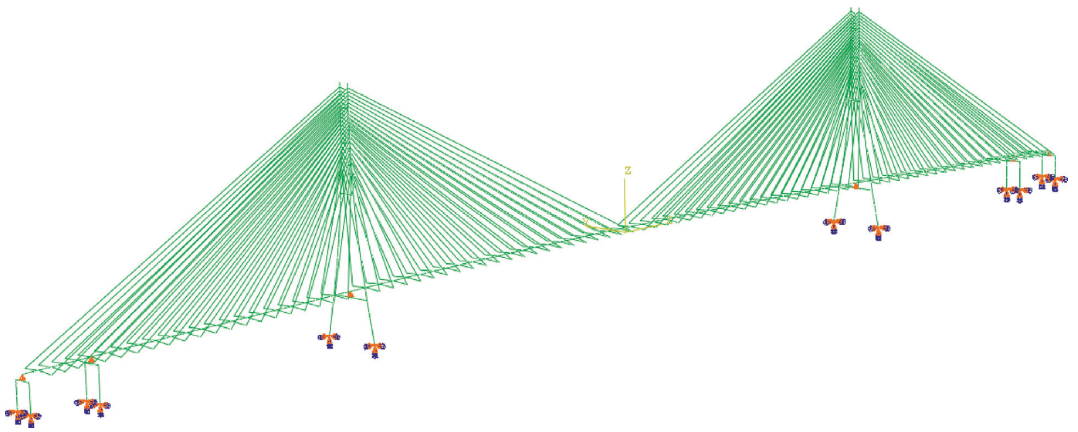

Figure 9: 3D finite element model.

Table 2: Structural model parameters.

Component name	Materials	Geometric parameters	Coefficient of thermal expansion (/°C)
Steel box girder	Q345D	3.2 m height and 37.2 m width (including wind fairing)	1.2×10^{-5}
Stay cable	High-strength low relaxation steel wire	109 to 241 wire, 7 mm diameter	1.36×10^{-5}
Steel pylon	Q370qD	170.8 m height; hollow rectangular cross section with 6.8 m × 5.0 m	1.2×10^{-5}
Main piers	C50 concrete	35.2 m height; Section with 12 m × 8.4 m	1.0×10^{-5}
Auxiliary pier	C40 concrete	Separated rectangular cross section hollow piers; 30m height	1.0×10^{-5}
Transition pier	C40 concrete	Separated rectangular cross section hollow piers; 24.8 m and 28.8 m height	1.0×10^{-5}

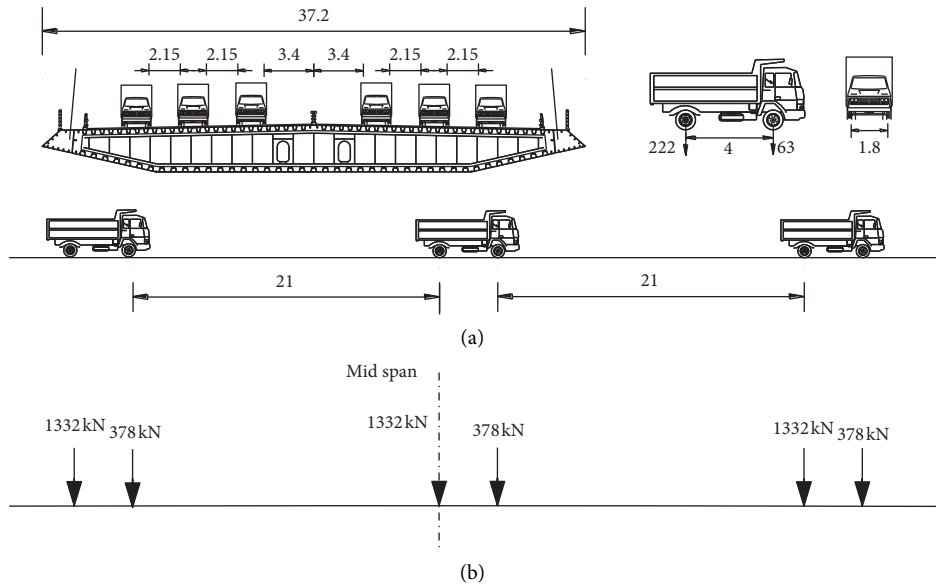

Figure 10: Comparison of truck loads in actual bridge and model: (a) truck deployment and (b) loads on model (unit: m).

according to the geometric parameters and material properties listed in Table 2 [25–30].

A spatial beam element was adopted for the steel box girder, main pylon, and pier; a tension-only truss element was employed for the stay cable. Rigid arm connection was adopted between the node and stay cable. The mass of the diaphragm plate and deck pavement was defined by nodal loads. The constraint conditions of the whole bridge included consolidation of the main tower bottom, the auxiliary pier bottom, and the transition pier bottom in this case. The vertical and horizontal supports between the main beam and the tower column were simulated by a spring element with a certain rigidity. The effect of cable sag cannot be considered in a simulation of a cable with a truss element, so we imposed an equivalent elastic modulus method on the cable with an Ernst formula. Our ABAQUS initial finite element model of the whole cable-stayed bridge contains 5,515 nodes and 3,805 elements. The cable sag effect was considered in the nonlinear analysis.

This bridge was modified with a combined static and dynamic model. A loading test was conducted on the completed bridge to validate the model by comparison against the simulation results. Eighteen trucks (63 kN front axle, 222 kN back axle weight) were placed in the mid-span area resulting in a load arrangement as shown in Figures 10(a) and 10(b) for the actual bridge and the model, respectively.

Table 3 gives measurement and calculation results. The statistical items included 19–21# cable forces at the river side of the south pylon, mid-span deflection, and vertical one-order frequency. Among them, the average relative error of the three cable forces is −1.7%.

4.2. Comparison of Finite Element Simulation and Monitoring Results. Accurate temperature simulation was crucial in this study for an effective contrast between the calculated and measured values. The unit temperature action was imposed on the model according to the actual measured temperature gradient of the girder as shown in Table 4; Table 4 also gives the calculated values of the mid-span deflection under different temperature actions. Figure 11 shows the girder deflection variations under four types of thermal actions. They indicate that the positive temperature gradient of the

Table 3: Comparison of measuring and calculated values.

Monitoring positions	Calculated values in model (kN)	Measured values (kN)	Relative error (%)
Cable 21#	457.8	465.8	−1.7
Cable 20#	482.0	507.0	−4.9
Cable 19#	465.9	459.4	1.4
Mid-span deflection	42.9	44.3	3.2
Vertical one-order frequency	0.2619	0.2637	−0.7

Table 4: Calculated values of mid-span deflection under different temperature actions.

Name of temperature actions	Values applied in the model (°C)	Calculated values (mm)
Temperature rise of the whole structure	1	−1.59
Temperature difference between cable and girder	0.5	8.99
Positive temperature gradient of girder	1	28.74
Positive temperature gradient of pylon	1	0.04

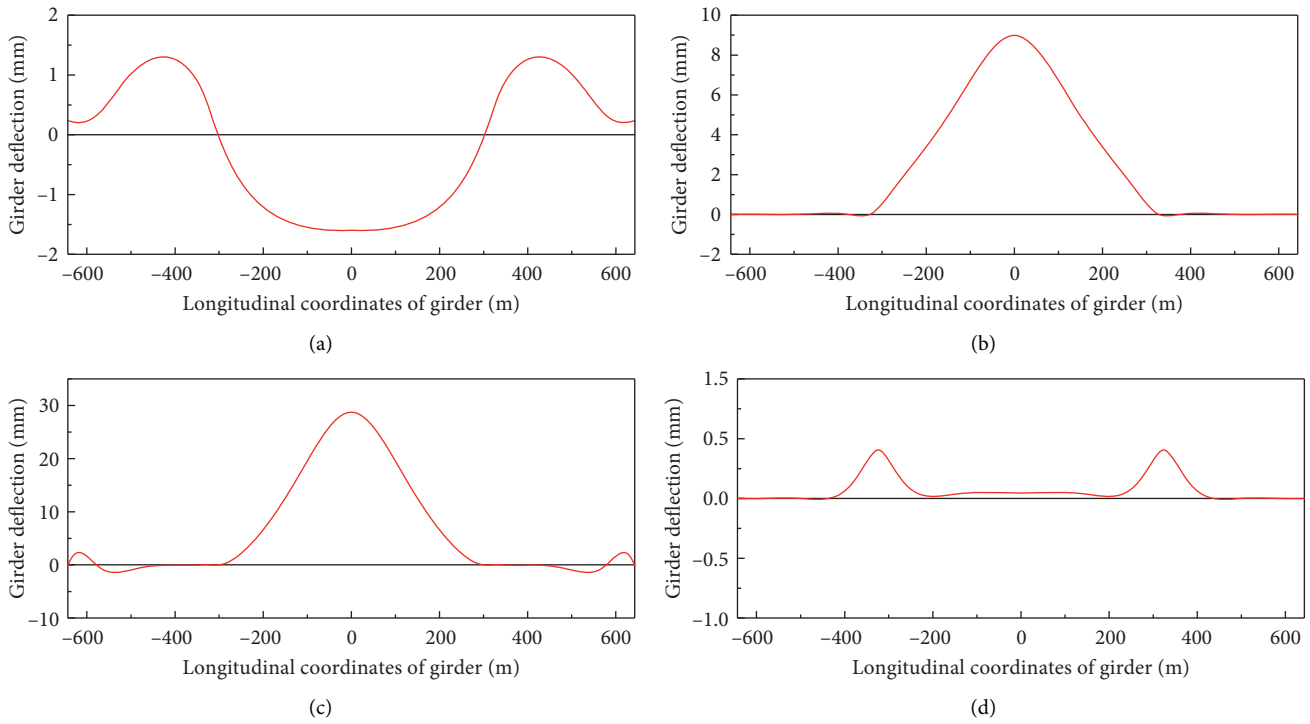

Figure 11: Girder deflection variation under four types of thermal actions. (a) The temperature rise of the whole structure. (b) Temperature difference between cable and girder. (c) Positive temperature gradient of girder. (d) Positive temperature gradient of pylon.

girder and temperature difference between the cable and girder appear to be the strongest influence on the mid-span deflection among all the factors observed here. The overall temperature change of the whole structure is relatively large and changes in a manner opposite to these two effects. The influence of the temperature gradient of the pylon on the mid-span deflection is negligible.

It is worth noting that uniform temperature variations were input to the model for analysis. That is to say, the spatial variations in temperature and effects of sunlight radiation were not considered (as was the case in a previous study [26]). This is not especially problematic for steel bridge analyses but may affect the results for concrete bridges or members.

The results of finite element simulation and actual monitoring for the deflection change behavior on different time scales are as follows.

4.2.1. Diurnal Variations. In the diurnal deflection variations, the monitoring data is greatly affected by one-day temperature differences and solar radiation. The bridge is mainly affected by the temperature difference between the cable and beam and the temperature gradient of the girder under solar radiation. The calculated sum of these two is 37.73 mm per degree Celsius; the monitoring fitting data is roughly 40 mm per degree Celsius. The finite element results accurately fit the changes in monitoring data. The influence

of solar radiation fluctuates in severity, so the hysteresis loops are different sizes and the changes are nonlinear.

4.2.2. Annual Variations. The annual variations in deflection are mainly affected by the increases and decreases in overall temperature across the structure. The monitored deflection rate with temperature is −1.721 mm per degree Celsius and the finite element simulation result is −1.6 mm per degree Celsius; these values are very similar.

The above results suggest that the finite element simulation we conducted effectively describes the deflection changes under different temperatures in the target bridge. Detailed analysis of such results can provide bridge maintainers with accurate, comprehensive bridge deformation information to make effective judgments regarding damage in the bridge.

5. Conclusions

Our conclusions based on time multiscale effect analysis of deflection in a steel cable-stayed bridge with temperature variations can be summarized as follows:

(1) The girder temperature gradient and the tower temperature gradient in current Chinese codes cannot be reasonably applied to steel box girders in steel cable-stayed bridges. However, the monitoring value of the bridge analyzed in this study conforms to the temperature gradient under British code. The girder temperature gradient of British standard BS 5400 can thus be reasonably applied for finite element simulation. The tower temperature gradient must be fitted with measurement data.

(2) The time scale variations in girder deflection are both diurnal and annual. Diurnally, the deflection is greatly affected by the temperature difference between the cable and beam and the temperature gradient of the girder. The annual variation law of deflection data and temperature at 1 : 00 am presents obvious linear characteristics. These phenomena were corroborated by finite element simulation.

(3) The daily deflection at 1 : 00 am can be unified to a certain reference temperature. This deflection index reflects the long-term degradation law of the structure, which provides an approach for efficient and rapid mining of massive sets of monitoring data.

(4) This work remits a deeper understanding of the multiscale behavior characteristics of deflection in steel cable-stayed bridges. However, our conclusions are limited to steel box girder cable-stayed bridges with steel towers and are not necessarily applicable to other types of cable-stayed bridges or bridges at alternate sites.

Data Availability

The data used to support the findings of this study are available from the corresponding author upon request.

Conflicts of Interest

The authors declare that there are no conflicts of interest regarding the publication of this paper.

Acknowledgments

This research was financially supported by the National Natural Science Foundation of China (No. 51808301) and Zhejiang Natural Science Foundation (No.LQ19E080006). This work was also sponsored by K. C. Wong Magna Fund at Ningbo University.

References

[1] G. M. Guzman-Acevedo, G. E. Vazquez-Becerra, J. R. Millan-Almaraz et al., "GPS, accelerometer, and smartphone fused smart sensor for SHM on real-scale bridges," *Advances in Civil Engineering*, vol. 2019, Article ID 6429430, 9 pages, 2019.

[2] H. Wang, T. Tao, A. Li, and Y. Zhang, "Structural health monitoring system for sutong cable-stayed bridge," *Smart Structures and Systems*, vol. 18, no. 2, pp. 317–334, 2016.

[3] J. M. W. Brownjohn, K.-Y. Koo, A. Scullion, and D. List, "Operational deformations in long-span bridges," *Structure and Infrastructure Engineering*, vol. 11, no. 4, pp. 556–574, 2015.

[4] M. T. Yarnold and F. L. Moon, "Temperature-based structural health monitoring baseline for long-span bridges," *Engineering Structures*, vol. 86, pp. 157–167, 2015.

[5] S.-H. Kim, S.-J. Park, J. Wu, and J.-H. Won, "Temperature variation in steel box girders of cable-stayed bridges during construction," *Journal of Constructional Steel Research*, vol. 112, pp. 80–92, 2015.

[6] Y. Fu and J. T. DeWolf, "Effect of differential temperature on a curved post-tensioned concrete bridge," *Advances in Structural Engineering*, vol. 7, no. 5, pp. 385–397, 2004.

[7] J.-H. Lee and I. Kalkan, "Analysis of thermal environmental effects on precast, prestressed concrete bridge girders: temperature differentials and thermal deformations," *Advances in Structural Engineering*, vol. 15, no. 3, pp. 447–459, 2012.

[8] B. Gu, Z.-j. Chen, and X.-d. Chen, "Temperature gradients in concrete box girder bridge under effect of cold wave," *Journal of Central South University*, vol. 21, no. 3, pp. 1227–1241, 2014.

[9] W. Gaoxin and D. Youliang, "Research on monitoring temperature difference from cross sections of steel truss arch girder of dashengguan yangtze bridge," *International Journal of Steel Structures*, vol. 15, no. 3, pp. 647–660, 2015.

[10] P. Yan, "Research on temperature field and temperature stress of large span concrete cable-stayed bridge girder," *Applied Mechanics and Materials*, vol. 178-181, pp. 2075–2080, 2012.

[11] Y.-L. Ding and G.-X. Wang, "Estimating extreme temperature differences in steel box girder using long-term measurement data," *Journal of Central South University*, vol. 20, no. 9, pp. 2537–2545, 2013.

[12] J. Reilly and B. Glisic, "Identifying time periods of minimal thermal gradient for temperature-driven structural health monitoring," *Sensors*, vol. 18, no. 3, p. 734, 2018.

[13] Y. Cao, J. Yim, Y. Zhao, and M. L. Wang, "Temperature effects on cable stayed bridge using health monitoring system: a case study," *Structural Health Monitoring*, vol. 10, no. 5, pp. 523–537, 2011.

[14] J. Lee, S. P. Chang, H. Kim, and J. G. Yoon, "Statistical time series analysis of long-term monitoring results of a

cable-stayed bridge," in *Proceedings of the 3rd International Conference on Bridge Maintenance, Safety and Management - Bridge Maintenance, Safety, Management, Life-Cycle Performance and Cost*, pp. 187-188, Porto, Portugal, 2006.

[15] Y. Zhu, Y. Fu, W. Chen, and S. Huang, "Online deflection monitoring system for dafosi cable-stayed bridge," *Journal of Intelligent Material Systems and Structures*, vol. 17, no. 8-9, pp. 701–707, 2006.

[16] L. Zhou, Y. Xia, J. M. Brownjohn, and K. Y. Koo, "Temperature analysis of a long-span suspension bridge based on field monitoring and numerical simulation," *Journal of Bridge Engineering*, vol. 21, no. 1, Article ID 04015027, 2016.

[17] Y. Zhou and L. Sun, "A comprehensive study of the thermal response of a long-span cable-stayed bridge: from monitoring phenomena to underlying mechanisms," *Mechanical Systems and Signal Processing*, vol. 124, pp. 330–348, 2019.

[18] J.-M. Lucas, M. Virlogeux, and C. Louis, "Temperature in the box girder of the normandy bridge," *Structural Engineering International*, vol. 15, no. 3, pp. 156–165, 2005.

[19] Y. Xia, B. Chen, and Y. L. Xu, "Temperature monitoring of tsing ma suspension bridge: numerical simulation and field measurement," *Earth and Space Engineering, Science, Construction, and Operations in Challenging Environments*, pp. 2535–2542, 2010.

[20] C. Miao and C. Shi, "Temperature gradient and its effect on flat steel box girder of long-span suspension bridge," *Science China Technological Sciences*, vol. 56, no. 8, pp. 1929–1939, 2013.

[21] Y. Zhou, L. Sun, and Z. Peng, "Mechanisms of thermally induced deflection of a long-span cable-stayed bridge," *Smart Structures and Systems*, vol. 15, no. 3, pp. 505–522, 2015.

[22] BS 5400: Part2, *Steel Concrete and Composite Bridges*, Specifications for loads., 1978.

[23] D. 60-2015 JTG, *General Specifications for Design of Highway Bridges and Culverts (In Chinese)*, People's Communications Press Co., Ltd., Beijing, China, 2015.

[24] T. Guo, J. Liu, Y. Zhang, and S. Pan, "Displacement monitoring and analysis of expansion joints of long-span steel bridges with viscous dampers," *Journal of Bridge Engineering*, vol. 20, no. 9, Article ID 04014099, 2015.

[25] Y. Ding, T. Yan, Q. Yao, X. Dong, and X. Wang, "A new type of temperature-based sensor for monitoring of bridge scour," *Measurement*, vol. 78, no. 78, pp. 245–252, 2016.

[26] N. Tayşi and S. Abid, "Temperature distributions and variations in concrete box-girder bridges: experimental and finite element parametric studies," *Advances in Structural Engineering*, vol. 18, no. 4, pp. 469–486, 2015.

[27] J. Zhu and Q. Meng, "Effective and fine analysis for temperature effect of bridges in natural environments," *Journal of Bridge Engineering*, vol. 22, no. 6, Article ID 04017017, 2017.

[28] J. Lee, K. C. Lee, and Y. J. Lee, "Long-term deflection prediction from computer vision-measured data history for high-speed railway bridges," *Sensors*, vol. 18, no. 5, p. 1488, 2015.

[29] W.-S. Liu, G.-L. Dai, and S.-C. Rao, "Numerical calculation on solar temperature field of a cable-stayed bridge with U-shaped section on high-speed railway," *Journal of Central South University*, vol. 21, no. 8, pp. 3345–3352, 2014.

[30] L. E. Rodriguez, P. J. Barr, and M. W. Halling, "Temperature effects on a box-girder integral-abutment bridge," *Journal of Performance of Constructed Facilities*, vol. 28, no. 3, pp. 583–591, 2014.